Contents lists available at ScienceDirect

Applied Catalysis B: Environmental

Evolution of unburnt hydrocarbons under "cold-start" conditions from adsorption/desorption to conversion: On the screening of zeolitic materials

Alexandre Westermann [a], Bruno Azambre [a,*], Gisèle Finqueneisel [a], Patrick Da Costa [b], Fabien Can [c]

[a] Université de Lorraine, Laboratoire de Chimie et Physique Approche Multi-échelle des Milieux Complexes (LCPA2MC), EA 4632, Institut Jean Barriol, Rue Victor Demange, 57500 Saint Avold, France
[b] Sorbonne Universités, UPMC Univ. Paris 06, Institut Jean Le Rond d'Alembert, CNRS UMR 7190, 2 place de la gare de ceinture, 78210 Saint Cyr l'École, France
[c] Institut de Chimie des Milieux et Matériaux de Poitiers IC2MP, UMR 7285 CNRS, Université de Poitiers, 4 rue Michel Brunet, 86022 Poitiers, France

ARTICLE INFO

ABSTRACT

The general purpose of this work is to examine the relative ability of some well-selected zeolitic materials for the reduction of HC emissions generated within the Diesel "cold-start" period, i.e. when the work temperature of the Diesel Oxidation Catalyst (DOC) has not been reached. More peculiarly, this study is focused on the chemical, textural and structural parameters of zeolites influent on the elimination, namely by adsorption, of unburnt HC (propene, toluene and decane) in presence of potential inhibitors (H_2O, CO, NO). Simulated "cold-start" conditions consisted in the rapid heating of the pre-treated zeolite sorbent/catalyst under the whole gas mixture from 35 to 530 °C. The quantity of trapped HC and those converted to CO_x by oxidation were measured in function of the temperature, as well as the amount of NO_x converted by the HC-SCR reaction. The interpretation of the HC emission profiles in close relation with the porous and acidic (through FTIR of adsorbed pyridine) properties of the corresponding zeolites allowed to gain insight onto the relative contributions of the pore topology, the pore size and the acid strength. For some selected zeolites, several consecutive cold-start cycles were performed in order to assess their stability.

© 2014 Elsevier B.V. All rights reserved.

1. Introduction

Environmental regulations on unburnt hydrocarbons (HC) emitted from mobile sources are becoming worldwide increasingly demanding. In the case of diesel light vehicles, most of these HC emissions are effectively converted to harmless products by an on-board Diesel Oxidation Catalyst (DOC), when the temperature of exhaust gases exceeds its light-off temperature (typically 200–300 °C) [1]. However, 80% of the residual HC pollution is still produced under "cold-start conditions", i.e. during the first two minutes (or even for a shorter period if a close-coupled catalyst is present) of the driving cycle [1,2]. HC in exhaust gases include branched and linear alkanes, alkenes, oxygenates and aromatics of various molecular weights, ranging from C_1 to C_{16}.

Further reduction of these HC emissions can be performed with the help of close-coupled or electrically heated catalysts but one of the most promising after-treatment technology consists in trapping the unburnt HC onto a sorbent at low temperatures. Within this concept, the HC-trap has to assist the Diesel Oxidation Catalyst (DOC) during the cold-start period i.e. when the exhaust temperature is below the light-off temperature of the DOC. Once this light-off temperature is reached, the trapped HC may eventually desorb and can be effectively oxidized by the DOC, so that the trap can be regenerated.

For a practical application, the following requirements have to be fulfilled: (i) an effective trap is targeted to adsorb most of the HC present in the exhaust, without showing significant selectivity for a given class of compounds; (ii) adsorption has to be strong enough in order to prevent the release of some HC at too low temperatures; (iii) the HC-trap has to be resistant to potential inhibitors present in exhaust gases, namely water, but also CO_x, NO_x and SO_x; (iv) the trapping material (in washcoated form) should be re-used for

* Corresponding author. Tel.: +33 387939106; fax: +33 387939101.
E-mail address: bruno.azambre@univ-lorraine.fr (B. Azambre).

Table 1
Structural, textural and chemical characteristics of the used zeolites.

Samples	Structure Pore size (Å)	Si/Al	S_{BET} (m^2 g^{-1})	S_{ext} (m^2 g^{-1})	S_{micro} (m^2 g^{-1})	Acidity (μmol g^{-1})[a,b]		
						Lewis	Brönsted	Total
Ca5A	LTA (5.0 × 5.0)	2	430	301	129	n.d	n.d	n.d
HMOR-20	MOR (6.5 × 7.0)	20	525	170	355	24	277	301
HZSM5-11	MFI (5.3 × 5.6 5.1 × 5.5)	11.5	310	5	305	45	273	318
Hβ-25	*BEA (5.6 × 5.6 6.6 × 7.6)	25	650	215	435	146	120	266
HY-100	FAU (7.4 × 7.4)	100	735	36	699	8	16	24
HY-15		15	835	30	805	43	71	114
HY-5		5.1	756	61	695	137	172	309
Pt-3/Y			660	64	596	126	143	269
Cu-9.5/Y			615	63	542	543	82	625

[a] Determined by pyridine adsorption followed by IR spectroscopy (evacuation at 150 °C).
[b] Determination not possible for Ca5A zeolite.

many adsorption/desorption cycles and should therefore present sufficient mechanical and heat resistance.

About these last two issues, it has been shown for instance that the much studied Cu-ZSM-5 zeolite is not suitable for automotive applications due to structural damages induced by the presence of steam at elevated temperatures and loss of active copper component. Furthermore, the strong exotherm induced by the combustion of adsorbed hydrocarbons was also found to promote this instability. Nevertheless and owing to the possibility of finely tuning their structural, textural and chemical parameters, zeolites still represent an obvious choice for the design of such a HC-trap. Furthermore, zeolites loaded with transition or precious metals can be by themselves effective oxidation or HC-SCR catalysts.

Literature studies addressing all these issues simultaneously are surprisingly missing and relevant data on the adsorption of HC mixtures in absence/presence of inhibitors are scarce or incomplete. The present study aimed to fill this gap. For that purpose, a screening of several zeolitic adsorbents was carried out under simulated "cold-start" conditions. These conditions consist in performing heating cycles under a well-defined gaseous mixture of HC (propene (C_3), toluene (C_7), decane (C_{10})) and inhibitors (water, CO and NO) and measuring continuously the emissions of HC, CO_x and NO_x at the reactor outlet.

Several characteristics of the zeolitic materials were investigated: (i) the type of structure (FAU, LTA, *BEA, MOR, MFI were used); (ii) the Si/Al ratio (for the Faujasite structure); (iii) the nature of the compensating cation (Cu, Pt, for the Faujasite structure).

2. Experimental

2.1. Materials

All the commercial zeolites used in this study (with different structures and framework molar Si/Al ratio ranging from 5 to 100, see Table 1 for further details) were provided by Zeolyst either in ammonium or protonated forms, excepted HY-100 and Ca5A, which were supplied by Degussa and Aldrich, respectively. Prior to use, the supports were calcined under air (4 L/h/g) with a heating rate of 5 °C/min from room temperature to 200 °C (plateau of 1 h) and then to 500 °C (plateau of 4 h). This procedure allowed to obtain all the zeolites in protonated forms while preserving their structure from damages caused by desorbing water.

Pt and Cu-modified zeolites (Table 1) were prepared by means of two different synthesis routes. Pt-3 wt%/Y zeolite was prepared by incipient wetness impregnation of HY-5 support using the adequate amount of a PtCl$_2$ precursor salt. Cu-9.5 wt%/Y zeolite was prepared by three successive ionic exchanges of HY-5 support at 60 °C for 2 h using a 0.05 M copper acetate (CuAc) solution at pH = 5 (allowing an exchange-degree of 140%). In both cases, the modified

zeolites were carefully dried at 80 °C and calcined under nitrogen flow at 500 °C prior to characterization and cold-start tests.

2.2. Characterizations

Porosimetric properties were obtained from N_2 adsorption isotherms recorded at −196 °C on an automated Autosorb-IQ sorptiometer supplied by Quantachrome. Prior to each adsorption measurement, samples were outgassed in situ in vacuum at 80 °C for 3 h and then at 150 °C for 12 h to remove any adsorbed impurities. Specific surface area (S_{BET}) was determined using the BET equation while microporous and external surface area were computed using the t-plot method [3].

Powder X-ray diffraction (PXRD) measurements were carried out using a Brüker-AXS diffractometer and the CuKα radiation (1.5405 Å). Powdered diffraction patterns were recorded between 5 and 50° (2θ) using increments of 0.01° and a counting time of 2 s.

Acidic properties were characterized by pyridine (Py) adsorption monitored by infrared spectroscopy. IR spectra were recorded on a Nicolet Nexus spectrometer equipped with a DTGS detector and a KBr beamsplitter using a resolution of 4 cm^{-1} and 64 scans. Samples were progressively activated under nitrogen flow (30 mL min^{-1}) up to 200 °C (5 °C/min) for 30 min and then to 450 °C (5 °C/min, 30 min). Pyridine was then adsorbed (200 Pa at equilibrium) at 25 °C and further desorbed until 150 °C. The total amount of Brönsted (BAS) and Lewis (LAS) Acid Sites were determined from the area of the ν19b mode (at 1545 cm^{-1} for BAS and 1450 cm^{-1} for LAS), using their molar coefficient (ε_{PyH+} = 1.8 cm μmol^{-1} and ε_{PyL} = 1.5 cm μmol^{-1}) respectively [4]. Finally, the spectra obtained on the different samples were normalized to a disc of 10 mg cm^{-2} in order to obtain quantitative results.

2.3. Cold-start tests

A cold-start test (CST) consists to a cycle performed under a representative gaseous mixture that is close to the real one experienced by an on-line HC-trap (presence of inhibitors and reactive gases) in an automobile [2]. Due to the rapid heating during the cycle, adsorption/desorption processes (with the gaseous mixture described below) take place simultaneously and the sorbent is never saturated with HC species (non-equilibrated adsorption). O_2 and NO_x being also present in the feed gas, HC oxidation and NO_x reduction are also expected to occur during the heating, as it will be shown later on.

More peculiarly, CST experiments were performed in a fixed-bed reactor (with EUROTHERM 2408 temperature controller and a K-type thermocouple), using 0.2 g of zeolite loaded into a U-type (internal diameter = 6 mm) glass cell between 2 plugs of quartz wool. To ensure a reproducible feed at the reactor inlet, the concentration of each species was set-up using mass-flow controllers
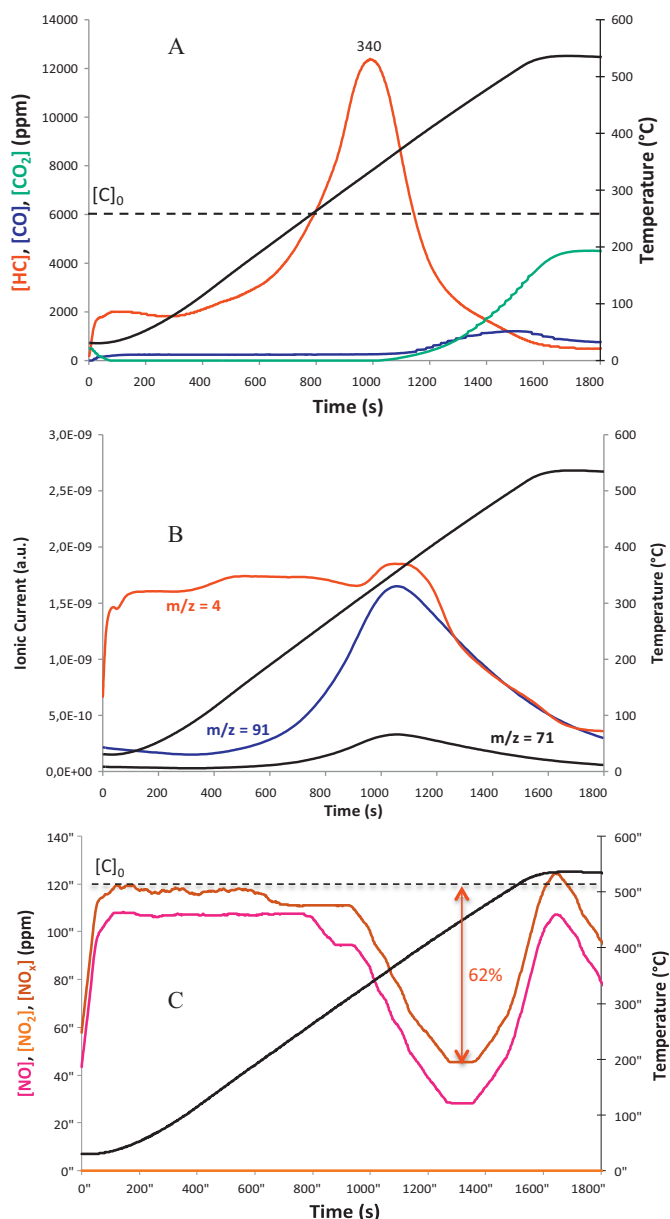
Fig. 1. (A) HC (FID signal) and CO_x emission profiles; (B) MS data and (C) NO, NO_2 and NO_x profiles monitored for HMOR-20 zeolite during a single CST cycle under a gaseous mixture composed by: 670 ppm propene, 280 ppm toluene and 200 ppm decane (the sum corresponding to the dotted line – 6000 ppm HC equiv. C_1), 125 ppm NO, 250 ppm CO, 10% O_2 and 3% H_2O (balance Ar). Temperature programme: 35–530 °C (v = 20 °C/min).

(Brooks, model 5850 TE), bubble towers set to well-defined temperatures (45 °C for decane and water; 5 °C for toluene), and heated transfer lines at 120 °C. In each experiment, the gaseous mixture was constituted by: 6000 ppm equiv. C_1 of HC (670 ppm propene, 280 ppm toluene and 200 ppm decane; each HC concentration being equal to 2000 ppm equiv. C_1), 125 ppm NO, 250 ppm CO, 10% O_2 and 3% H_2O (balance Ar). The total flow rate was maintained at 250 mL min^{-1} (GHSV = 20,000 h^{-1}). Prior to apply the temperature programme (heating ramp from 35 to 530 °C with v = 20 °C/min) in presence of this gaseous mixture, the concentrations were allowed to equilibrate in a bypass. Hence, the initial (t_0) points in the experiments presented in CST profiles (Figs. 1 and 2) correspond to the time when the feed gas was sent from the bypass to the adsorbent.

The concentrations of the different compounds exiting the reactor were continuously monitored using different detectors. An Eco Physics CLD 700 AL chemiluminescence NO_x analyzer (for NO and total NO_x allowed to the simultaneous detection of NO and NO_x (NO_2 by difference). Two Ultramat 6 IR analyzers were used to monitor N_2O, CO and CO_2. A FID detector (Fidamat 5) was used to measure the total concentration of the HC compounds. Specific profiles corresponding to each HC were monitored through a Pfeiffer Vacuum GSD 301 Quadrupole Mass Spectrometer (MS) using the following signals: propene (m/z = 42), toluene (m/z = 91) and decane (m/z = 71).

Because the stability of the sorbent material is an important issue for a practical application, some selected zeolites (HY-5, HY-100, Pt-3/Y and Cu-9.5/Y) were selected to undergo 4 consecutive CST cycles.

3. Results and discussion

3.1. General description of the accessible pore structure for the investigated zeolites

Up to 5 zeolite framework types have been used in this work (see Table 1). The structural data of our commercial zeolites, as deduced from their corresponding XRD patterns (not shown here), were found to be consistent with the expected ones [4–8].

Our general aim being to establish relationships between the pore topology, pore size and acidity on the one hand, and the CST results on the other hand, the different structures were arbitrarily classified in three groups depending on the pore topology accessible to HC molecules:

(i) The LTA (Ca5A) and FAU (HY, Si/Al = 5, 15, 100) structures are composed by sodalite cages linked together by d4R units and hexagonal prisms, respectively. The particular arrangement of these sodalite cages forms α cages (also called supercages due to their size, approximately 11.8 Å in diameter). Supercages are linked together through windows of 5 (LTA) or 7.4 Å (FAU), and this forms the accessible pore network (due to their molecular size, the HC used in this study can not diffuse through the empty spaces leading to the sodalite cages).

(ii) The framework of *BEA (Hβ-25) structure displays a system of two interconnected channels (straight and zigzag). These two channels have a pore diameter of 5.6 Å × 5.6 Å and 6.6 Å × 7.6 Å, respectively. The framework of HZSM5-11 zeolite (structure MFI) can be regarded as roughly similar to the one of the *BEA structure, but the pore size is smaller with 5.3 Å × 5.6 Å and 5.1 Å × 5.5 Å in diameter.

(iii) The framework of MOR (HMOR-20 zeolite) can be considered as a one-dimensional pore system, with a pore size of 6.5 Å × 7.0 Å.

3.2. Textural characterization

The porosimetric characteristics (S_{BET}, S_{ext} and S_{micro}) summarized in Table 1 indicate that the specific surface area of the different zeolites depend namely on their structural type and spread between 310 m^2 g^{-1} for HZSM5-11 and 835 m^2 g^{-1} for HY-15. Rather consistently, large-pore zeolites (HMOR-20, HY-15 and Hβ-25) having 12 membered-ring channels or windows also display the highest S_{BET} and S_{micro}. By contrast, zeolites with 8 or 10 membered-ring openings (HZSM5-11 and Ca5A) have lower specific surface area (Table 1). Only, the Ca5A, HMOR-20 and Hβ-25 zeolites display significant contributions of their external surfaces (301, 170 and 215 m^2 g^{-1}, respectively) to the overall specific surface area.

Among the series constituted by HY zeolites with three different Si/Al ratios (5, 15 and 100), no specific order was observed about the
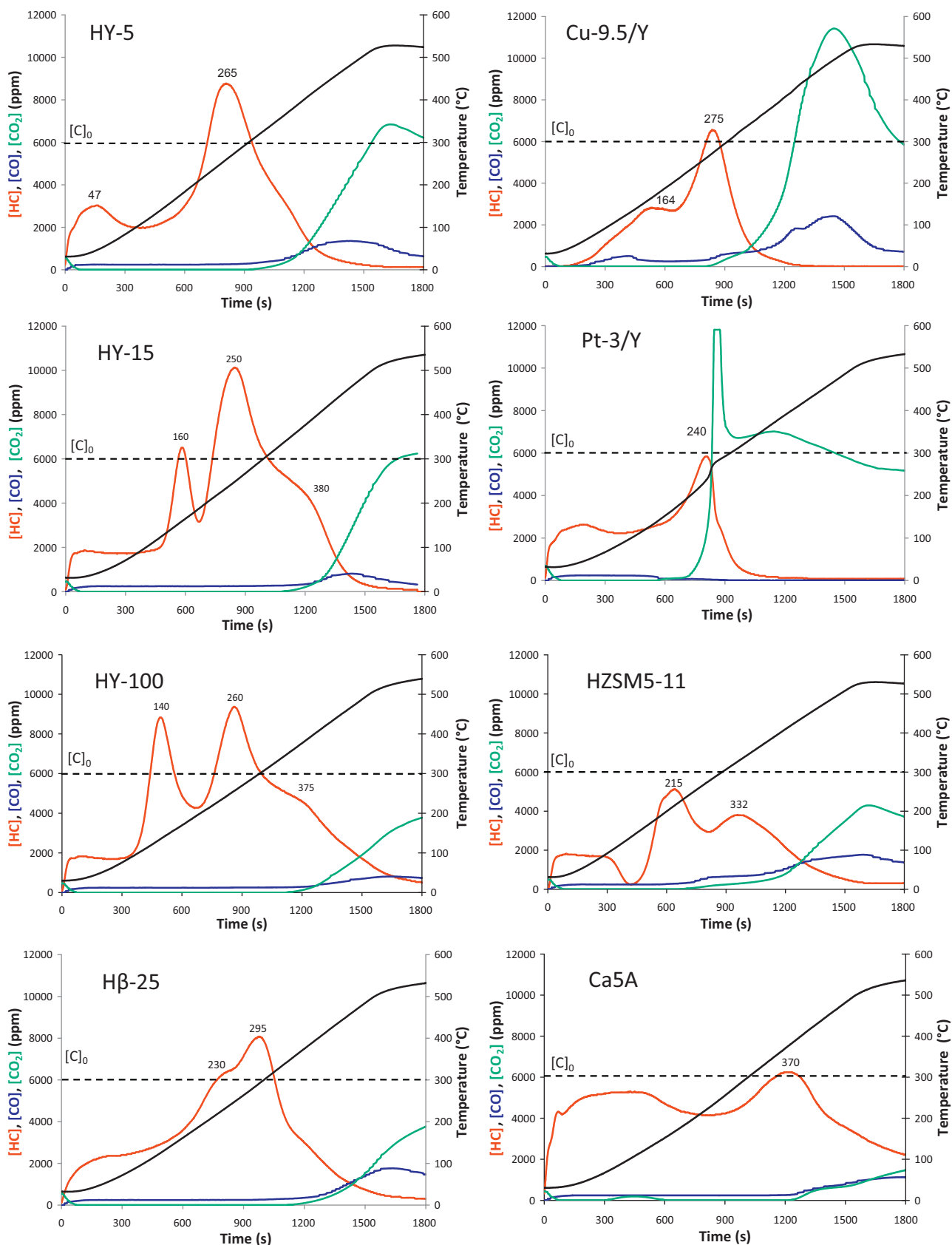
Fig. 2. HC (FID signal) and CO_x emission profiles monitored for the different studied zeolites during the first CST cycle under a gaseous mixture composed by: 670 ppm propene, 280 ppm toluene and 200 ppm decane (the sum corresponding to the dotted line – 6000 ppm HC equiv. C_1), 125 ppm NO, 250 ppm CO, 10% O_2 and 3% H_2O (balance Ar). Temperature programme: 35–530 °C ($v = 20$ °C/min).

evolution of the porosimetric characteristics. On the other hand, the specific surface area of HY-5 decreases by 13% after impregnation with $PtCl_2$ (from 756 to 660 m² g⁻¹) and by 19% after successive ionic exchange with Cu^{2+} (from 756 to 615 m² g⁻¹), respectively. For the Pt-3/Y sample, this decrease has to be explained by to the partial blockage of the Faujasite porous network after impregnation, due to the accumulation of some metallic species at the 12 membered-ring windows or at the pore mouth [9]. Concerning the Cu-exchanged zeolite, the decrease of the S_{BET} and S_{micro} may be caused by the presence of less dispersed species after the last exchange, as suggested by Diaz et al. [10]. When the exchange degree exceeds 100%, an accumulation of copper ions is expected, which is in line with the present experimental data.

3.3. Acidity studies from FTIR of adsorbed pyridine

In zeolites, Brönsted acid sites correspond to the bridged Si-OH-Al groups and their amount and strength depend on the Si/Al atomic ratio [11]. Thermal treatments and dealumination procedures used in the syntheses of the different zeolites can partially remove aluminium from the crystal framework. It is assumed that, the aluminium removed from the framework remains in the cavities (extra-framework aluminium, or EFAL) as nanoparticles whose surface induces Lewis acidity, which can be quantified by pyridine adsorption for instance. With the aim of measuring the acidity of the different zeolites both qualitatively and quantitatively, pyridine was preferred to ammonia as molecular probe because its dimensions (kinetic diameter equal to 5.8 Å [12]) better match with those of the adsorbed HC (propene = 4 Å [13], toluene = 5.8 Å [14] and decane = 4.3 Å [13]). Hence, only the sites potentially accessible to the HC were probed by FTIR of adsorbed pyridine (see part 2 for experimental details). In Table 1 are given the concentrations of Lewis and Brönsted acid sites as well as the total acidity (both in µmol g⁻¹) for each zeolite [15].

Among the different structural types investigated (with Si/Al ratio in the 11–25 range), HMOR-20 and HZSM5-11 display the highest concentrations of Brönsted acid sites (Si(OH)Al hydroxyls) with ~275 µmol g⁻¹, i.e. about twice those found for Hβ-25 and four times more than for HY-15. These trends are overall consistent with those reported in the literature [15–19]. In addition, some Lewis acidity was observed for all samples. Its origin is presumably due to the presence of extra-framework aluminium debris brought by thermal or dealumination processes. Still within the series composed by the different structural types, the Hβ-25 zeolite possesses the highest amount of Lewis acid sites ~140 µmol g⁻¹, with the following order obtained: Hβ-25 ≫ HY-15 ~ HZSM5-11 > HMOR-20. Here, it is possible that the high Lewis acidity of the Hβ-25 zeolite arises from the low crystallinity of this material and/or from the possible co-existence of several BEA* polymorphs (as deduced from the existence of broad peaks in its XRD pattern). On the other hand, the above classification could not be applied for zeolite Ca5A because of its pore size incompatible with pyridine and the presence of very strongly adsorbed water (that could not be evacuated) in the micropores.

Among the series constituted by HY zeolites, it clearly appears that, the lower the Si/Al ratio (in the range 5–100), the higher the total amount of acid sites (both of Brönsted and Lewis types, Table 1). Moreover, it can be established that our HY-5 zeolite has acidic properties rather comparable to Hβ-25 in terms of concentrations of Brönsted acid sites and aluminic extra framework debris (Lewis acid sites).

As deduced from Table 1, the successive ion-exchange procedures of HY-5 with Cu^{x+} cations led to a decrease of the Brönsted acidity by a factor 2 while strongly increasing the Lewis acidity (from 137 to 543 µmol g⁻¹ for Cu-9.5/Y). The additional Lewis acid sites are due to the presence of Cu^{2+} and Cu^+ cations in $S_{I'}$, S_{II} and $S_{II'}$ positions ([20–26], as also revealed by DRIFTS of adsorbed NO and CO, not shown here) and also possibly to very small clusters not detectable by XRD. By contrast, the impregnation of the Pt salt has a negligible effect on the acidic properties of the parent zeolite (Table 1), and metallic Pt^0 particles located on the external surface of the crystallites were detected for the Pt-3/Y zeolite by XRD, confirming the results of Chakarova et al. [27].

3.4. General interpretation of a cold-start test (CST): case of the HMOR zeolite

Since many zeolites were used in this study, the in-depth presentation and interpretation of CST data will be limited to a single zeolite only, for the sake of brevity. In the later sections, only the differences of behaviour between the different zeolitic materials will be outlined and commented in detail.

In Fig. 1A, are displayed the total HC and CO_x emission profiles in the case of the HMOR-20 zeolite. The specific temperature profiles corresponding to the emission of each individual HC (propene (m/z = 42), toluene (m/z = 91) and decane (m/z = 71)), as monitored from Mass Spectrometry, are given in Fig. 1B whereas Fig. 1C represents the evolution of N-containing products (NO, NO_2, N_2O and total NO_x).

Starting from Room Temperature, a plateau in the FID profile corresponding to ca 2000 ppm equiv. C_1 (Fig. 1A) is detected almost immediately. According to the SM data displayed in Fig. 1B, these HC emissions have to be assigned exclusively to propene, which is not adsorbed on most of the zeolites used in this study (including HMOR-20), with some exceptions that will be put forward later on. The non-adsorption of propene in presence of other HC and inhibitors (water, CO, NO) is in strong contrast with the results obtained by Lopez et al., who measured a significant propene adsorption capacity of 26 mg/g on a Na-MOR zeolite under single-adsorption conditions [1]. Hence, it can be hypothesized that either the presence of the heavier HC or the inhibitors may be responsible of these discrepancies. In that respect, some studies have reported that the mordenite structure is rather unselective for the adsorption of different HC present in a mixture [28]. Hence, it seems reasonable that the water molecules present in rather large amounts in the feed gas (3%) are the main inhibitors for propene, due to an adsorption competition onto the same acid sites [29–32].

Most of the "missing" HC (area below the $[C_0]$ line) at low temperatures (35–250 °C, Fig. 1A) are therefore due to the storage of toluene and decane in the straight channels of the HMOR-20 zeolite. The simultaneous occurrence of desorption processes is visible from the increase of HC emissions, starting from ca 100 °C, up to 340 °C (maximum). MS data (Fig. 1B) reveal that toluene and decane are desorbed simultaneously on HMOR-20. The reported HC adsorption mechanism on zeolites of Mordenite-type, known also as "single-file diffusion" [28], is thought to involve first the strong adsorption of toluene in the straight channels of the unidimensional structure, which is promoted by the high acid strength of the HMOR-20 zeolite and the presence of many acid sites (see Table 1). Toluene adsorbed molecules act as plugs for the decane molecules intercalated between them. Hence, decane molecules cannot escape the channels until toluene has desorbed, both processes taking place simultaneously.

Above 340 °C, HC emissions progressively decline due to: (i) oxidation processes, as witnessed by the detection of significant amounts CO and CO_2 in the gas phase (Fig. 1A); (ii) the occurrence of coking reactions (for a minor part) revealed by the darkening of the sample. Though the HC oxidation mechanism is beyond the scope of this study, it may involve the activation of molecular oxygen by Brönsted acid sites as a first step [33]. At 530 °C, all the incoming or desorbing HC are converted to CO_x on HMOR-20 zeolite (CO_2/CO = 4, Table 2).

Table 2

Desorption temperature maxima, amount of CO_x emitted, CO_2/CO ratio, percentage of hydrocarbon trapped, percentage of hydrocarbon eliminated, DeNO$_x$ window and NO$_x$ conversion to N$_2$ determined from a single CST cycle.

Samples	Desorption T (°C)	n_{CO_x} (mmol/g)	CO_2/CO	HC trapped[a] (%)	HC eliminated[b] (%)	DeNO$_x$ window (°C)	NO$_x$ conversion to N$_2$ (%)
Ca5A	120, 370	0.65	1.6	4	20	260–500	53
Hβ-25	230, 295	1.30	1.9	36	47	160–500	52
HMOR-20	340	1.75	4.0	56	36	315–500	63
HZSM5-11	215, 332	2.50	2.1	62	64	120–500	81
HY-100	160, 240, 375	0.23	∞	18	29	340–450	12
HY-15	160, 250, 380	2.1	11.0	32	43	110–250 390–490	25
HY-5	47, 265	2.91	5.3	44	53	165–270 350–450	47
Pt-3/Y	47, 240	5.35	∞	43	71	120–300	42
Cu-9.5/Y	164, 275	5.40	5.8	69	75	300–530	63

[a] Net percentage of hydrocarbons trapped ($\%_{adsorbed} - \%_{desorbed}$) onto the adsorbent between 35 and 250 °C.

[b] Percentage of hydrocarbons eliminated as CO_2 and/or coke between 35 and 530 °C.

To sum up the behaviour of HMOR-20 concerning its reaction with HC, it can be noted that the percentage of HC eliminated (the major part by oxidation and a minor part by coking) over the entire CST cycle (from 35 to 530 °C) is 36% (Table 2 and Fig. 3B). More interestingly, the percentage of HC trapped by sorption from 35 to 250 °C represents 56% of the total amount of HC sent on the catalyst over the same temperature range (Table 2 and Fig. 3A). We will refer to this parameter later on as "trapping efficiency". The trapping efficiency is of particular significance for a practical implementation because the HC re-emitted at temperatures above 250 °C can be completely oxidized by a DOC (for instance a Pt-supported material) placed downstream in the exhaust line.

Another parameter of interest is the elimination of NO$_x$ during a CST cycle. In Fig. 1C, the NO$_x$ concentration at the reactor outlet remains overall equal to the C_0 value below 300 °C and then passes to a minimum at 450 °C. In absence of any detected NO$_2$ and N$_2$O, it can be calculated that 62% of the incoming NO$_x$ are reduced to N$_2$ at this temperature, the "DeNO$_x$" window spreading between 315 and 500 °C. The production of N$_2$ occurs through HC-SCR reactions catalyzed by the HMOR-20 zeolite. It is expected that either the stored HC or their cracking products act as reducing agents for NO$_x$, the active sites for NO reduction to N$_2$ being the protons or still, some Al^{3+} defects [34].

3.5. Comparison between the CST behaviour of the different zeolites

In Fig. 2, are compared the total HC and CO$_x$ (CO and CO$_2$) emission profiles recorded during a CST cycle for the different zeolites investigated. The trapping efficiencies, defined thereafter as the total sum of HC stored below 250 °C, are compared in Fig. 3A, whereas the fractions of HC eliminated (as COx and/or coke) over a whole CST cycle (between 35 and 530 °C) are given in Fig. 3B. The temperature profiles of NO, NO$_2$, Total NO$_x$ and N$_2$O are also compared in Fig. 4. Complementary quantitative informations useful for a fine characterization of each zeolite behaviour are summarized in Table 2.

In order to make the discussion easier, groups of zeolites were distinguished and analyzed separately, according to the Si/Al ratio, the nature of the cation and the type of structure.

3.5.1. Effect of the Si/Al ratio

The first group is constituted by HY zeolites with increasing Si/Al ratio (5, 15 and 100). Whatever the Si/Al ratio, propene is not adsorbed in presence of inhibitors on HY zeolites, excepted slightly for the most acidic one, HY-5. By contrast with the CST profile of HMOR-20 (Fig. 1), the FID profile of HY-100 is more complex with the presence of two well-separated peaks (Fig. 2). As deduced from SM data (not shown here), the first one at 140 °C is related to the emission of a weakly-held form of toluene, while the second at 260 °C and the shoulder at 375 °C are namely due to the desorption of decane. Oligomers and cracking products arising from secondary reactions of decane (and toluene disproportionation) with strong acid sites also contribute to the second (high-temperature) peak. Interestingly, it is worth noting that the temperature of the toluene desorption peak follows a trend opposite to that of the Si/Al ratio. Hence, the single broad and unresolved peak observed at 260 °C for HY-5 (Fig. 2) corresponds both to the desorption of decane and a strongly held form of toluene. The HY-15 zeolite displays an intermediate behaviour, the separation between the low- and high-temperature peaks being still visible, though narrower than for HY-100. These evolutions can be rationalized by considering the existence of a higher amount of acid sites when the Si/Al ratio decreases (Table 1). For HY-5, toluene molecules have more chance
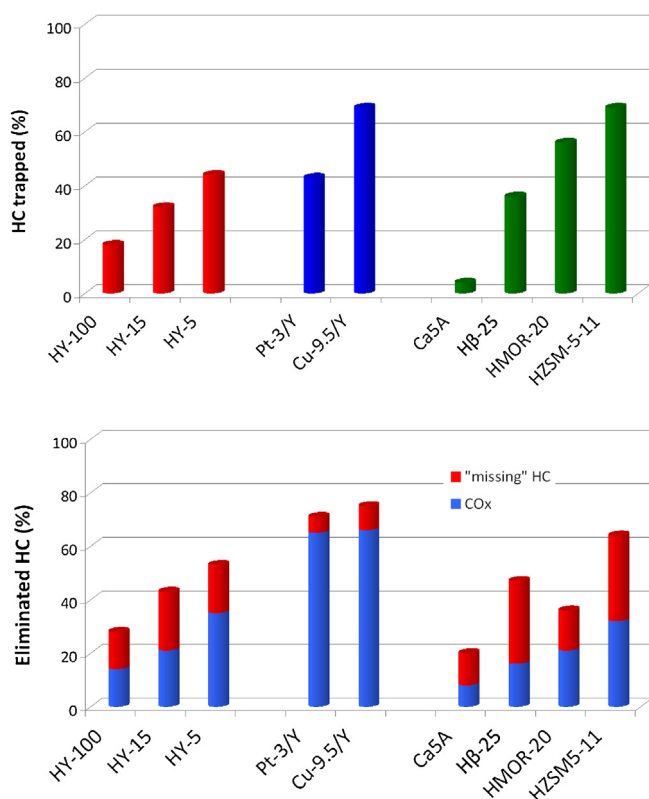

Fig. 3. (A) Trapping efficiencies corresponding to the fractions of HC trapped below 250 °C; (B) fractions of HC eliminated over a whole CST cycle (from 35 to 530 °C). The fraction eliminated as CO$_x$ is indicated in blue. The term "missing HC" refers to the fraction of HC that was either deposited as coke or that could not be quantified.
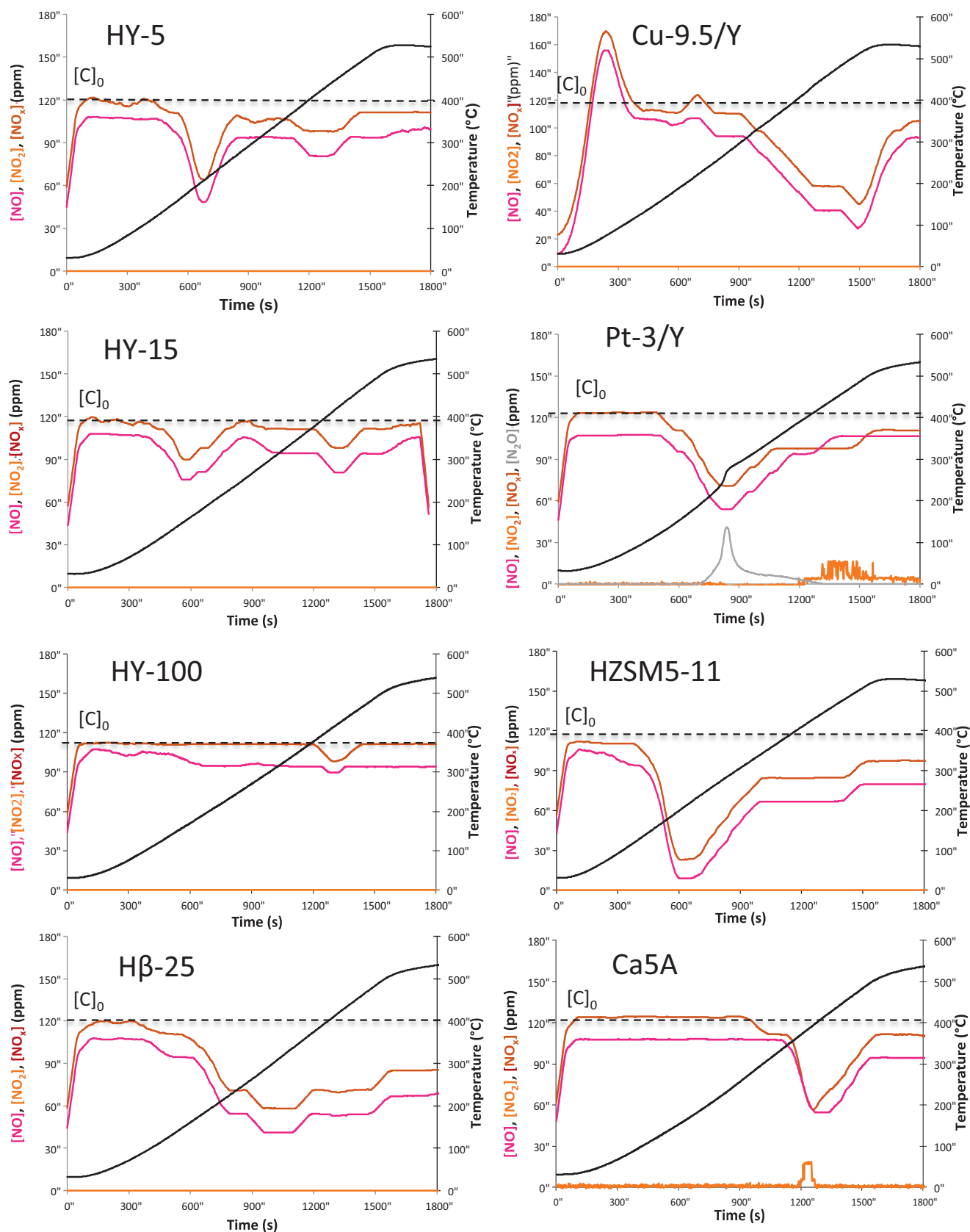
Fig. 4. NO, NO_2, total NO_x and N_2O profiles monitored during a single CST cycle for the different studied zeolites under a gaseous mixture composed by: 670 ppm propene, 280 ppm toluene and 200 ppm decane (the sum corresponding to the dotted line – 6000 ppm HC equiv. C_1), 125 ppm NO, 250 ppm CO, 10% O_2 and 3% H_2O (balance Ar). Temperature programme: 35–530 °C ($v = 20$ °C/min).

to interact strongly with acid sites because the density of these sites within the Y framework is considerably higher than for HY-100. In that respect, it is well known that the preferred siting of toluene consists in interactions between Lewis acid sites and the aromatic ring whereas hydrogens of the methyl group point towards the zeolite framework oxygens [35]. In the lack of available acid sites, dispersive (weak) interactions with the pore walls eventually occur and this interaction mode should predomine at the high Si/Al ratio. This explains the trends observed for the adsorption of toluene on the series constituted by HY zeolites.

Still within the same series, it is worth noting that the global trapping efficiency below 250 °C (Fig. 3A) decreases with the Si/Al ratio, passing from 44% for HY-5 to only 18% for HY-100. Interesting trends are also observed concerning the transient HC oxidation to CO_x (Fig. 3B) and NO_x conversions to N_2 (Fig. 4) Considering the catalyzed HC oxidation to CO_x first, CO_2 is detected from 300 °C for HY-5, whereas the onset of oxidation is delayed to 340 °C for HY-15 and 350 °C for HY-100 (Fig. 2). It is worth noting that the total sum of HC eliminated and CO_x produced over a CST cycle follow the same trend: HY-5 > HY-15 > HY-100 (Fig. 3B). Hence, it can be concluded that the ability of the HY zeolites to oxidize the HC depend on their relative acidities in the Si/Al range 5–100 (Table 1), the most acidic one (HY-5) having both the best trapping efficiency and also the best oxidizing properties.

Coming now to the reduction of nitrogen oxides, two windows of NO_x conversion to N_2 are visible (Fig. 4). The first "DeNO$_x$" window is centred at *ca* 200 °C (zeolites HY-5 and HY-15), whereas the second is at 430 °C (all HY zeolites). From the results of Fig. 4, it seems clear that the amounts of NO_x converted to N_2 at these temperatures are somewhat correlated to the availability and strength of acid sites (Brönsted and Lewis) on the different zeolites through their Si/Al ratio. Here again, the following order is obtained: HY-5 > HY-15 > HY-100. Acid sites are not only involved in the dissociation of NO to N_2, but are also expected to contribute to some crucial steps of the DeNO$_x$ mechanism, such as the NO oxidation to NO_2, and/or the secondary reactions of the trapped HC with the NO_2 formed [34]. About the latter, it has been reported that cracked products or molecular fragments (such as CH_x entities from decane cracking) can often be considered as better reductants than their parent HC.

3.5.2. Effect of the charge-compensating cation

The incorporation of metallic species into the HY-5 zeolite by impregnation (Pt-3/Y) or ion-exchange (Cu-9.5/Y) induces some obvious changes on the CST behaviour (Fig. 2).

Interestingly, the Cu-9.5/Y zeolite displays a zero HC emission profile during the first 200 s, meaning that all types of HC, including propene, are adsorbed on this catalyst. By comparison with the parent HY-5 zeolite (Fig. 2), a new emission peak is detected at 164 °C, corresponding to the desorption of propene adsorbed at lower temperatures on Cu^{x+} sites. Among the different zeolitic materials investigated, it is worth noting that only the copper-exchanged Y zeolite was able to trap propene significantly in presence of the other HC and the inhibitors. This seems consistent with the fact that Ag$^+$ and Cu$^+$ cations at exchangeable positions have the ability to efficiently activate double bonds of many types of molecules [35,36]. As summarized in Fig. 3A, the enhanced adsorption of unsaturated HC on Cu-9.5/Y accounts for its high trapping efficiency (69%, Fig. 3A), the highest of all the zeolites investigated. By contrast, the Pt-3/Y zeolite displays a trapping efficiency similar to that of the parent zeolite (44%).

By contrast with HY-5, Cu-9.5/Y and more peculiarly Pt-3/Y display much less HC emissions in the 250–530 °C range, due to the occurrence of oxidations reactions promoted by metal sites. For the Pt-3/Y material, the brutal combustion of the stored HC is responsible of both the exotherm and the very sharp CO_2 peak visible at *ca*

240 °C (Fig. 2). Above this temperature, all the incoming HC and CO (present as 250 ppm in the feed) undergo a total (catalytic) oxidation to CO_2 (and H_2O), these processes being catalyzed by the Pt^0 crystallites located on the HY external surface. Hence, the Pt-3/Y can be considered to have a "DOC-like" behaviour. By contrast, the Cu-9.5/Y has less oxidizing properties, as witnessed for instance by the existence of residual CO emission at 530 °C (end temperature of CST cycle). Nevertheless, the amounts of HC converted to CO_x on Cu-9.5/Y are much higher than for the parent HY-5 zeolite. Consistently with their enhanced oxidation properties, the Cu- and Pt-containing Y zeolites display the highest fractions (about 70–75%) of HC eliminated over a whole CST cycle of all the zeolites investigated (Fig. 3B).

As expected from their HC emission profiles, the Cu- and Pt-containing zeolites displayed also NO_x reduction features widely different from those observed for the parent HY-5 zeolite (Fig. 4). The Pt-3/Y zeolite is characterized by a broad peak of NO_x conversion at low temperature (120–350 °C) and centred at *ca* 240 °C. Consistently, the peak temperature of NO_x conversion also corresponds to the brutal oxidation of the stored HC, while N_2O is simultaneously detected. At higher temperatures, the NO_x conversion quickly decline because all the incoming HC are fully converted to CO_2 and there is no more HC available to reduce the NO_x. This behaviour is typical of a supported oxidation catalyst containing metallic platinum particles [37]. By contrast, the Cu-9.5/Y zeolite exhibit very different NO_x conversion profiles (Fig. 4): (i) a NO desorption peak is observed at low temperature (<100 °C) assigned to Cu^{x+}-NO nitrosyls [23]; (ii) the low-temperature DeNO$_x$ peak at 200 °C observed for HY-5 becomes hardly visible; (iii) a broad DeNOx window is observed at medium-high temperatures (300–530 °C) with a maximal NO_x conversion to N_2 of 63% at 500 °C. In this study, it has been shown by FTIR of adsorbed pyridine that more than half of the protons were exchanged with Cu^{x+} species and that the amount of Lewis acid sites increased by a factor 3 (Table 1). Therefore, the changes observed in the proportion and nature of active sites affect the DeNO$_x$ mechanism: the low-temperature peak observed for HY-5 and HY-15 at 200 °C can now be attributed to HC-SCR reactions on H$^+$ sites, whereas the medium-high temperature peak involves DeNOx reactions on Cu^{x+} sites, and to a lesser extent Al^{3+} defects.

3.5.3. Effect of the structure

Some differences existing between the HY (5, 15, 100), Hβ-25, HZSM5-11, HMOR-20, and Ca5A zeolites in terms of pore topology and relative acidity were already outlined in Sections 3.1 and 3.3. As expected, significant different behaviours are observed in Fig. 2, when comparing the CST profiles of these materials.

The behaviour of both HY and HMOR zeolites during a cold-start test was already described in previous sections. Among all the zeolites investigated, the Ca5A zeolite displayed the highest HC emissions at low temperatures (Fig. 2), *i.e.* a very weak trapping efficiency (4%, Fig. 3A). In fact, the narrow windows in the LTA structure prevent the bulky toluene molecules to enter the porosity, as confirmed by MS data. Because propene is also weakly adsorbed, most of the missing HC at *T* < 350 °C are solely due to the storage of decane, whose curved conformation in the gas phase is compatible with the pore size. For the Ca5A material, the existence of two broad emission peaks at *ca* 150 and 380 °C reveal a dual adsorption, on the external and internal surfaces, respectively (Fig. 2). Decane oxidation only starts above 380 °C and is rather limited, as witnessed both by the weak amounts of CO_x detected (Fig. 2) and the CO_2/CO ratio close to 1 (Table 2). Simultaneously to decane desorption/cracking, a small window of NO_x conversion (to N_2 and NO_2) is detected around 400 °C (Fig. 4).

By comparison with Ca5A zeolite, the other zeolitic materials did not show phenomena of steric hindrance during exposition to the
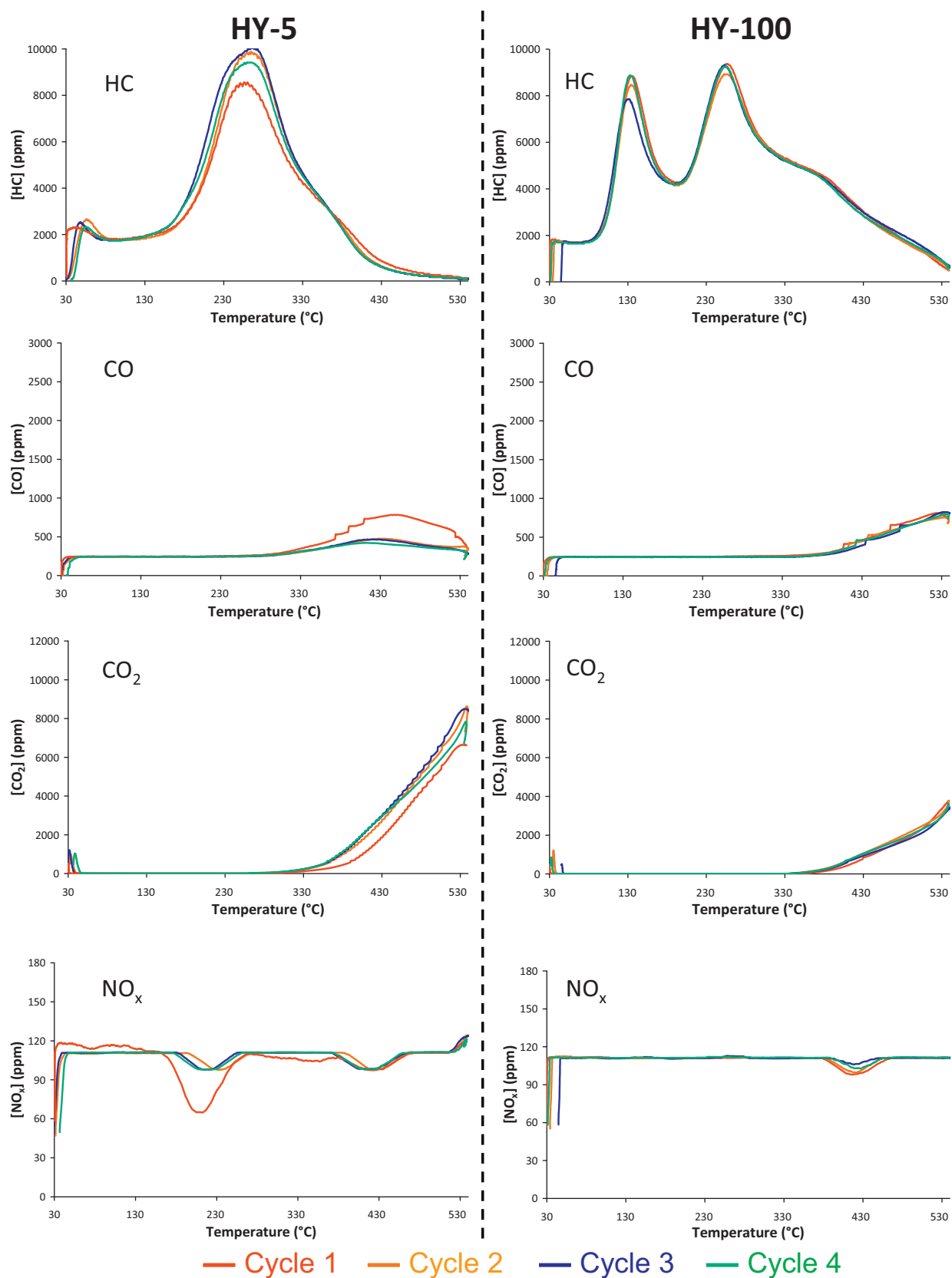
Fig. 5. Total HC, CO, CO_2 and NO_x emissions measured through 4 consecutive cold-start cycles for HY-5 (left) and HY-100 (right) zeolites.
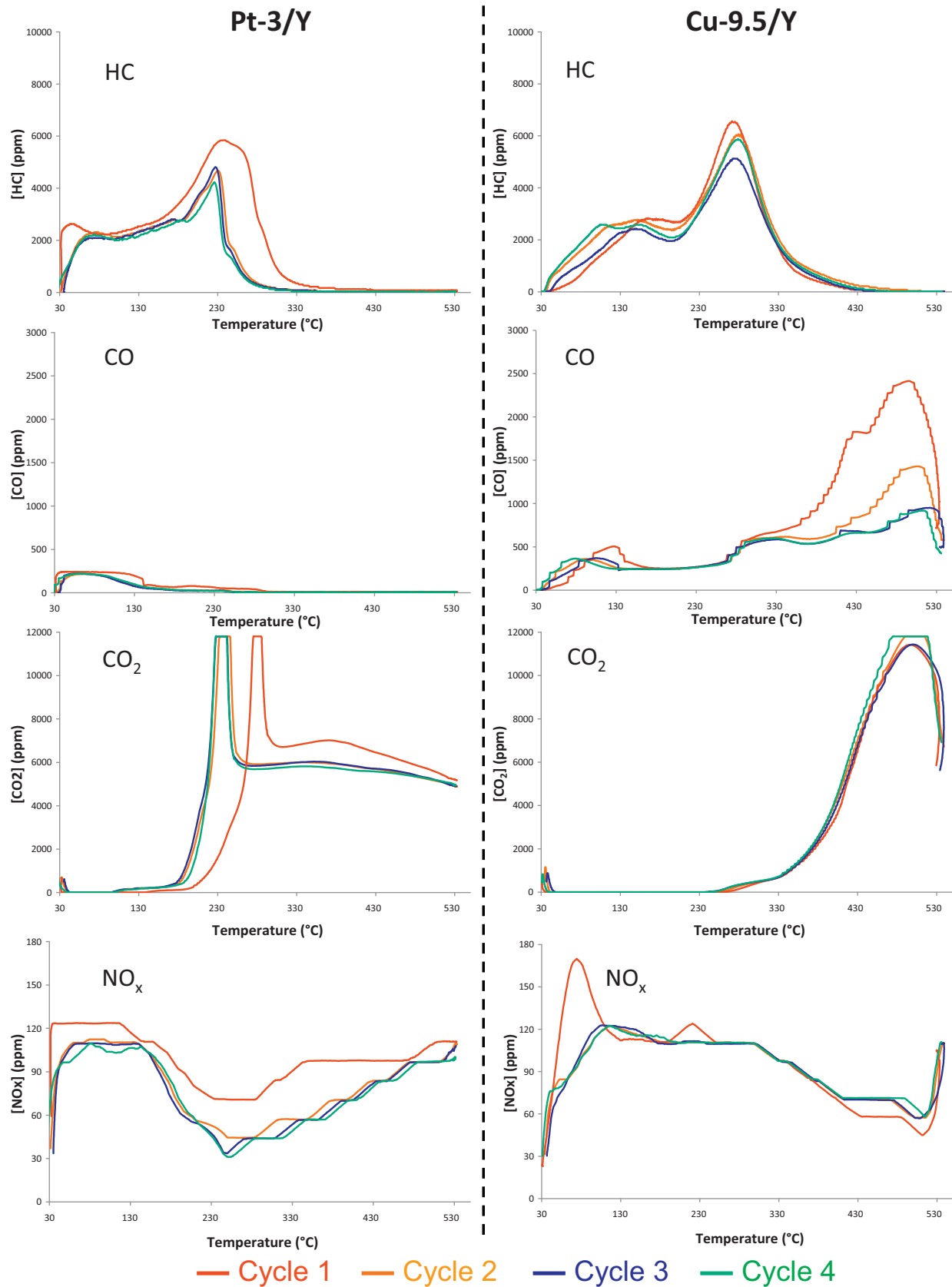
Fig. 6. Total HC, CO, CO_2 and NO_x emissions measured through 4 consecutive cold-start cycles for Pt-3/Y (left) and Cu-9.5/Y (right) zeolites.

HC mixture. Only Hβ-25 and HZSM5-11 were able to trap propene, however in much smaller amounts than for Cu-9.5/Y (Fig. 2). More peculiarly, the HZSM5-11 zeolite displays an unusual behaviour with all types of HC being suddenly trapped together in the course of the heating, at *ca* 130 °C (Fig. 2), whereas propene emissions were detected below this temperature. For the MFI structure, it can be recalled that toluene is preferentially adsorbed at the intersections between the straight and zigzag channels [38]. Its molecular size (5.6 Å) being rather comparable to those of the channels, its diffusion within the internal porosity is rather uncomfortable, especially at the lowest temperatures. Hence, it is possible that propene, which has been reported to adsorb mostly in the "zigzag" channels [38,39], is not able to enter them due to the blockage of intersections by toluene molecules. Overall, the CST behaviour of HZSM5-11 probably stands for an easier diffusion of the HC at the pore mouth or within the internal porosity of the MFI structure as the temperature increases. Another peculiarity of the HZSM5-11 zeolite lays in its ability to promote HC oxidation from *ca* 250 °C, a temperature much lower than for the other protonated zeolites (in most cases around 300–350 °C). As a result, only weak HC emission peaks are observed at 215 °C (toluene + decane) and 332 °C (decane, propene and cracking products) (Fig. 2). Also worth noting, the HZSM5-11 zeolite displays a strong NO_x conversion to N_2 of 81% at 220 °C and a low-medium NO_x conversion above 350 °C (Fig. 4).

Finally, the CST profile corresponding to Hβ-25 displayed two overlapping HC peaks, at 230 and 295 °C, respectively (Fig. 2). As deduced from MS data, these peaks have to be assigned mostly to decane, while the contributions of propene and toluene only slightly account for the second (high-temperature) peak. On this material, oxidation reactions start at 350 °C, and the CO_2/CO ratio was one of the lowest of all the zeolites investigated. Moreover, this material was found to be medium-active for the transient reduction of NOx, as witnessed by the broad $DeNO_x$ window, spreading between 160 and 500 °C, and the 52% conversion to N_2 at 320 °C (Fig. 4). The NO_x conversions observed at high temperatures have probably to be put in relation with the high amount of Lewis acid sites measured for this zeolite (Table 1).

In absence of steric limitations, the best trapping efficiencies were found for the most acidic zeolites, HMOR-20 and HZSM-11 with 56 and 62%, respectively, of HC trapped below 250 °C (Fig. 3A and Table 1). The fractions of HC eliminated over a whole CST cycle (Fig. 3B) are less informative, because a significant part of these HC is not converted to CO_x but rather to coke or other products.

3.6. Stability tests

Four zeolites were selected to undergo four consecutive CST cycles in order to assess their relative stability under cold-start conditions (Figs. 5 and 6).

In the series of HY zeolites (Fig. 5), the hydrophobic and non-acidic HY-100 zeolite was found to be the most stable concerning both the HC, CO_x and NO_x emission features, with no appreciable changes all along the different cycles. By contrast, an evolution was observed for the HY-5 zeolite (Fig. 5), namely between the first and second cycles (the material was found to be stable afterwards). During cycles 2–4: (i) propene is slightly better adsorbed; (ii) an increase of the amount of HC desorbed around 250 °C is observed; (iii) less CO and more CO_2 is produced at medium-high temperature; (iv) the NO_x conversion to N_2 at 200–220 °C decreases significantly. It is possible that the origin of these different behaviours arise from coking reactions, which are more likely to take place on the acidic HY-5 zeolite during the first CST cycle. Coke deposits may indeed influence the adsorption and diffusion of HC in the vicinity of acid sites, and affect the activity of H^+ sites in $DeNO_x$ reactions [40]. Also, they can slightly decrease the hydrophilicity

of the HY-5 internal surface, this being a promoting parameter for the adsorption of propene in presence of water.

The repetition of several CST cycles led to contrasted behaviours for the Pt-3/Y and Cu-9.5/Y zeolites (Fig. 6). Here also, the main changes are observed after the first cycle, the materials being rather stable afterwards.

Starting with the Pt-3/Y zeolite, it can established that: (i) the propene trapped at low temperature increases after cycle 1; (ii) HC oxidation reactions to CO_2 are promoted, resulting in lesser HC emissions; (iii) the NO_x conversion increases due to an enhanced oxidation of NO to NO_2 (above 230 °C) and more intense N_2O emissions (below 230 °C, not shown in Fig. 6). Thus, this reflects a change in the state of embedded platinum species, which occurs during the first CST cycle. Hence, the evolutions observed seem consistent with a further reduction and sintering of supported Pt particles, due to the presence of HC and/or water.

On the Cu-9.5/Y zeolite, propene and NO adsorptions, which were strongly promoted by Cu^{x+} sites at temperatures below 100 °C during the first cycle, are hindered in cycles 2–4 (Fig. 6). Also, significantly less CO emissions were detected above 350 °C and the NO_x conversion to N_2 is also negatively affected within the same temperature range. Though more investigations are needed to clarify the structural changes occurring in the catalyst, this probably points out a re-distribution and/or a partial reduction of Cu^{x+} sites after the first cycle.

4. Conclusions

In this study, a methodology was elaborated in order to investigate both qualitatively and quantitatively the behaviour of nine zeolitic materials under simplified conditions targeted to mimic those of diesel exhausts during the cold-start period (rapid heating from 35 to 530 °C under a mixture composed by 670 ppm propene, 280 ppm toluene, 200 ppm decane, 125 ppm NO, 250 ppm CO, 10% O_2 and 3% H_2O (balance Ar)).

The selected zeolites were characterized according to their structural, textural and acidic properties. The effects of some chemical parameters such as the Si/Al ratio or the nature of the charge-compensating cation were further evaluated for Y zeolites with Faujasite-type structure.

Namely, a "screening" of zeolites was performed according to their: (i) relative HC trapping properties at low temperatures; (ii) their ability in eliminating (namely by oxidation) the unburnt HC over a whole CST cycle; (iii) their performances in the Selective Catalytic Reduction (HC-SCR) of NO_x; (iv) their stability through several consecutive CST cycles.

The results showed that:

- The amounts of HC adsorbed under 250 °C overall increases with the acidity of zeolites, even in presence of inhibitors such as water, CO or NO. This is due mainly to the strong affinity of Brönsted acid sites and/or metallic species (exchanged Cu^{x+} cations, and Pt^0 nanoparticles) for the adsorption of unsaturated HC, such as propene and toluene. By contrast, weakly-acidic and/or hydrophobic zeolites (such as HY-100) are more selective for decane adsorption and are less interesting for cold-start applications;

- As expected, metal-loaded zeolites (namely with Pt) are the most efficient in oxidizing the trapped and/or incoming HC above 250 °C. Hence, they display the highest fractions of HC eliminated over a whole cold-start cycle. The Pt-3/Y zeolite is stable after one single CST cycle and has the typical behaviour of a Diesel Oxidation Catalyst. Though the HZSM5-11 zeolite has non-negligible HC oxidizing properties, zeolites in protonated forms are overall less efficient for HC oxidation and more subjected to coking;

- Among the zeolites investigated, the most acidic H^+/zeolites (such as HZSM5-11 and HMOR-20) and the Cu-9.5/Y zeolite display also the best transient NO_x conversion to N_2.

Though potentially interesting zeolitic materials were discovered in this study for cold-start applications, further investigations may be needed to find an optimized zeolitic material.

Acknowledgments

References

[1] J.M. Lopez, M.V. Navarro, T. Garcia, R. Murillo, A.M. Mastral, F.J. Varela-Gandia, D. Lozano-Castello, A. Bueno-Lopez, D. Cazorla-Amoros, Microporous Mesoporous Mater. 130 (2010) 239–247.
[2] J.H. Park, S.J. Park, I.S. Nam, G.K. Yeo, J.K. Kil, Y.K. Youn, Microporous Mesoporous Mater. 101 (2007) 264–270.
[3] B. Lippens, B. Linsen, J. de Boer, J. Catal. 3 (1964) 32–37.
[4] S. Khabtou, T. Chevreau, J.C. Lavalley, Micropor. Mater. 3 (1994) 133–214.
[5] A. Omegna, M. Vasic, J.A. van Bokhoven, G. Pirngruber, R. Prins, Phys. Chem. Chem. Phys. 6 (2004) 447–452.
[6] Y. Liu, W. Zhang, T.J. Pinnavaia, Angew. Chem. Int. Ed. 40 (2001) 1255–1258.
[7] D.W. Breck, Zeolite Molecular Sieves, Wiley, New-York, 1974.
[8] M.M.J. Treacy, J.B. Higgins, Collection of Simulated XRD Powder Patterns for Zeolites, Elsevier, New-York, 2001.
[9] P.A. Jacobs, J.B. Uytterhoeven, H.K. Beyer, J. Chem. Soc. Faraday Trans. 175 (1979) 56.
[10] E. Diaz, S. Ordonez, A. Vega, J. Copa, Appl. Catal. B 56 (2005) 313.
[11] E.M. Flanigen, H. Khatami, H.A. Szymanski, Molecular Sieve Zeolites-I – Advances in Chemistry, American Chemical Society, Washington, DC, 1974, 364 pp.
[12] L. Junlong, X. Huifu, H. Xiumin, W. Pei-Hao, H. Shing-Jong, L. Shang-Bin, S. Wenjie, Chin. J. Catal. 31 (2010) 729–738.
[13] R.M. Serra, E.E. Miro, P. Bolcatto, A.V. Boix, Microporous Mesoporous Mater. 147 (2012) 17–29.
[14] M.J. Lashaki, M. Fayaz, S. Niknaddaf, Z. Hashisho, J. Hazard. Mater. 241–242 (2012) 154–163.
[15] E.P. Parry, J. Catal. 2 (1963) 371.
[16] A. Hassan, S. Ahmed, M.A. Ali, H. Hamid, T. Inui, Appl. Catal. A 220 (2001) 59–68.
[17] M. Lashdaf, V.V. Nieminen, M. tiitta, T. Venäläinen, H. Österholm, O. Krause, Microporous Mesoporous Mater. 75 (2004) 149–158.
[18] H.M. Kao, C.Y. Yu, M.C. Yeh, Microporous Mesoporous Mater. 53 (2002) 1–12.
[19] T.K. Phung, M.M. Carnasciali, E. Finocchio, G. Busca, Appl. Catal. A 470 (2014) 72–80.
[20] J.H. Kwak, H. Zhu, J.H. Lee, C.H.F. Peden, J. Szanyi, Chem. Commun. 48 (2012) 4758–4760.
[21] P.A. Jacobs, H.K. Beyer, J. Phys. Chem. 83 (1979) 1174.
[22] P.A. Jacobs, W.D. Wilde, R.A. Schoonheydt, J.B. Uytterhoeven, H. Beyer, J. Chem. Soc. Faraday Trans. 72 (1976) 1221.
[23] J. Datka, P. Kozyra, J. Mol. Struct. 744–747 (2005) 991–996.
[24] G.T. Palomino, S. Bordiga, A. Zecchina, G.L. Marra, C. Lamberti, J. Phys. Chem. B 104 (2000) 8641.
[25] J. Szanyi, J.H. Kwak, H. Zhu, C.H.F. Peden, Phys. Chem. Chem. Phys. 15 (2013) 2368.
[26] K.I. Hadjiivanov, Catal. Rev. Sci. Eng. 42 (2000) 71–144.
[27] K. Chakarova, K. Hadjiivanov, G. Atanasova, K. Tenchev, J. Mol. Catal. A 264 (2007) 270–279.
[28] K.F. Czaplewski, T.L. Reitz, Y. JoongKim, R.Q. Snurr, Microporous Mesoporous Mater. 56 (2002) 55–64.
[29] J.H. Park, S. Jun Park, H.A. Ahn, I.S. Nam, G.K. Yeo, J.K. Kil, Y.K. Youn, Microporous Mesoporous Mater. 117 (2009) 178–184.
[30] T. Kanazawa, Catal. Today 96 (2004) 171–177.
[31] S.P. Elangovan, M. Ogura, S. Ernst, M. Hartmann, S. Tontisirin, M.E. Davis, T. Okubo, Microporous Mesoporous Mater. 96 (2006) 210–215.
[32] Z. Sarshar, M.H. Zahedi-Niaki, Q. Huang, M. Eic, S. Kaliaguine, Appl. Catal. B: Environ. 87 (2009) 37–45.
[33] J. Xu, B.L. Mojet, van OmmenF J.G., L. Lefferts, J. Catal. 232 (2005) 411–423.
[34] R. Bartolomeu, M. Foix, A. Fernandes, M. Tatoulian, M.F. Ribeiro, C. Henriques, P. Da Costa, Catal. Today 176 (2011) 234–238.
[35] R. Yoshimoto, K. Hara, K. Okumura, N. Katada, M. Niwa, J. Phys. Chem. C 111 (2007) 1474–1479.
[36] F. Benaliouche, Y. Boucheffa, F. Thibault-Starzyk, Microporous Mesoporous Mater. 147 (2012) 10–16.
[37] F. Diehl, J. Barbier Jr., D. Duprez, I. Guibard, G. Mabilon, Appl. Catal. B: Environ. 95 (2010) 217–227.
[38] D. Schuring, A.P.J. Jansen, R.A. van Santen, J. Phys. Chem. B 104 (2000) 941–948.
[39] A.O. Koriabkina, A.M. de Jong, D. Schuring, J. van Grondelle, R.A. van Santen, J. Phys. Chem. B 106 (2002) 9559–9566.
[40] C.J. Bennett, P.S. Bennett, S.E. Golunski, J.W. Hayes, A.P. Walker, Appl. Catal. A: Gen. 86 (1992) Ll–L6.